

A&A manuscript no.  
(will be inserted by hand later)

Your thesaurus codes are:  
06(08.19.5 SN 1987A; 02.14.1; 08.19.4)

ASTRONOMY  
AND  
ASTROPHYSICS

November 13, 2018

# ISO SWS/LWS observations of SN 1987A<sup>★</sup>

P. Lundqvist<sup>1</sup>, J. Sollerman<sup>1</sup>, C. Kozma<sup>1</sup>, B. Larsson<sup>1</sup>, J. Spyromilio<sup>2</sup>, A.P.S. Crotts<sup>3</sup>, J. Danziger<sup>4</sup>, and D. Kunze<sup>5</sup>

<sup>1</sup> Stockholm Observatory, SE-133 36 Saltsjöbaden, Sweden.

<sup>2</sup> European Southern Observatory, Karl-Schwarzschild-Strasse 2, D-85748 Garching, Germany.

<sup>3</sup> Columbia University, Dept. of Astronomy, 538 W. 120th Street, New York, USA

<sup>4</sup> Osservatorio Astronomico, Via G.B. Tiepolo 11, I-34131 Trieste, Italy.

<sup>5</sup> Max-Planck-Institut für extraterrestrische Physik, Postfach 1603, D-85740 Garching, Germany.

Received: 03 February 1999 Accepted: 14 April 1999

**Abstract.** We report on observations of SN 1987A with ISO SWS/LWS made 9 – 11 years after the explosion. No emission from the supernova was seen. In particular, the upper limits on the fluxes of [Fe I] 24.05 $\mu$ m and [Fe II] 25.99 $\mu$ m on day 3 999 are  $\sim 1.1$  Jy and  $\sim 1.4$  Jy, respectively. Assuming a homogeneous distribution of  $^{44}\text{Ti}$  inside 2000 km s<sup>-1</sup>, we have made theoretical models to estimate the mass of ejected  $^{44}\text{Ti}$ . Assessing various uncertainties of the model, we obtain an upper limit of  $\simeq 1.5 \times 10^{-4} M_{\odot}$ . The implications of this are discussed.

The LWS data display continuum emission as well as nebular lines of [O I], [C II] and [O III] from neighboring photoexcited regions in the LMC. The [O III] lines indicate an electron density of  $120 \pm 75$  cm<sup>-3</sup>, and the continuum can be explained by dust with a temperature of  $\sim 37$  K. A second dust component with  $\sim 10$  K may also be present.

**Key words:** supernova: individual: SN 1987A – nucleosynthesis – supernovae: general

## 1. Introduction

Supernova (SN) 1987A provides a convenient tool to test our understanding of nucleosynthesis in massive stars and during supernova explosions (Thielemann et al. 1996). In particular, the late ( $t \gtrsim 150$  days) emission probes directly the elemental abundances deep in the stellar ejecta. As in other core-collapse SNe without a dense circumstellar medium, the energy production is at this epoch dominated by radioactive energy from the decay of  $^{56}\text{Co}$  to  $^{56}\text{Fe}$ , the cobalt itself being the decay product of  $^{56}\text{Ni}$ . It was quickly realized that the ejected mass of  $^{56}\text{Ni}$  in SN 1987A was at least  $0.05 M_{\odot}$  (Woosley et al. 1988), the actual number

being close to  $0.07 M_{\odot}$  (e.g., Suntzeff & Bouchet 1990). This decay continued to power the bolometric light curve in an undisputed fashion for about  $\sim 800 - 1000$  days (Bouchet et al. 1996).

However, during the following epoch, radioactive decay seemed to be unable to explain the bolometric flux of the supernova, unless a large amount of  $^{57}\text{Ni}$  (decaying to  $^{57}\text{Co}$  and further to  $^{57}\text{Fe}$ ) was included (Suntzeff et al. 1992). Fransson & Kozma (1993) demonstrated that the derived  $^{57}\text{Ni}/^{56}\text{Ni}$  ratio could be much closer to the solar  $^{57}\text{Fe}/^{56}\text{Fe}$  ratio when time dependence was accounted for. This effect, now known as the “freeze-out” effect, stems from the fact that the energy stored at earlier epochs in the low-density hydrogen gas slowly leaks out and dominates the bolometric light curve after  $\sim 1000$  days (Fransson & Kozma 1999). The freeze-out effect becomes less important as the radioactive isotope  $^{44}\text{Ti}$  starts to dominate. This occurs after  $\sim 1500 - 2000$  days (Woosley et al. 1989; Kumagai et al. 1991; Fransson & Kozma 1999).  $^{44}\text{Ti}$  decays to  $^{44}\text{Sc}$  on a time scale of  $87.0 \pm 1.9$  years (Ahmad et al. 1998; Görres et al. 1998), and then quickly further to  $^{44}\text{Ca}$ .

It is important to determine the  $^{56}\text{Ni}$ ,  $^{57}\text{Ni}$  and  $^{44}\text{Ti}$  masses in order to constrain models for the supernova explosion and the explosive nucleosynthesis (e.g., Timmes et al. 1996). In the case of  $^{44}\text{Ti}$ , models predict that  $\sim 10^{-4} M_{\odot}$  could be synthesized in SN 1987A (e.g., Kumagai et al. 1991; Woosley & Hoffman 1991).

Chugai et al. (1997) estimate that the mass of ejected  $^{44}\text{Ti}$  should be  $M(^{44}\text{Ti}) \sim (1 - 2) \times 10^{-4} M_{\odot}$  from the optical line emission at 2875 days. Kozma (1999) and Kozma & Fransson (private communication 1999; hereafter KF99) preliminary find that  $M(^{44}\text{Ti}) = (1.5 \pm 1.0) \times 10^{-4} M_{\odot}$  best explains broad-band photometry of SN 1987A for  $t \lesssim 3270$  days. However, nearly all of the emission comes out in the far infrared which is not included in the observed bands. KF99 show that a more definite estimate can be made if one could measure the flux in a few iron lines, mainly [Fe II] 25.99 $\mu$ m. There are several reasons

<sup>★</sup> ISO is an ESA project with instruments funded by ESA Member States (especially the PI countries: France, Germany, the Netherlands and the United Kingdom) and with the participation of ISAS and NASA.

Correspondence to: peter@astro.su.se

**Table 1.** Log of observations.

Date	Phase <sup>a</sup>	Instrument/Mode	Exposure time <sup>b</sup>
96/05/26	3 380	SWS/AOT2	7 307
96/06/08	3 393	SWS/AOT2	2 545
97/07/19	3 799	SWS/AOT2	7 307
98/02/04	3 999	LWS/AOT1	3 641
98/02/04	3 999	SWS/AOT1	6 750

<sup>a</sup> Epochs in days past explosion.<sup>b</sup> Time in seconds.

for this. First, at  $\sim 4000$  days KF99 find that almost half of the luminosity from the supernova is emerging in this line. Second, because the iron lines are only little affected by freeze-out they are good tracers of the instantaneous energy deposition, and the flux of [Fe II] 25.99 $\mu$ m is therefore almost proportional to  $M(^{44}\text{Ti})$ . Third, this line is formed through collisional excitations and is therefore insensitive to uncertainties in atomic data involved in calculating the recombination cascade. In a preliminary analysis, Borkowski et al. (1997) find that their Infrared Space Observatory (ISO; Kessler et al. 1996) observations give an upper limit on the line flux which corresponds to only  $1.5 \times 10^{-5} M_{\odot}$ .

Here we report on observations we have made with ISO. Although we have observed the supernova over the entire wavelength range 2.38 – 197 $\mu$ m, we will concentrate our discussion on the region, 23 – 27 $\mu$ m, where the strongest emission lines are expected to emerge. We compare these observations with theoretical modeling. We also briefly discuss our observations at longer wavelengths where we detect emission originating from elsewhere in the LMC.

## 2. Observations and Results

We have used ISO to observe SN 1987A on several occasions. Both the Short Wavelength Spectrograph (SWS; de Graauw et al. 1996) and the Long Wavelength Spectrograph (LWS; Clegg et al. 1996) were used, and Table 1 summarizes our observations. We will concentrate here mainly on the SWS observation from 4 February, 1998 (Sect. 2.1), though we provide a consistency check of this observation against our other SWS observations. The LWS data are discussed in Sect. 2.2.

### 2.1. SWS Observations

The SWS observation on 4 February, 1998 was made in the SWS01 mode with speed 4 and was centered on the position of SN 1987A, i.e., R.A. = 5h 35m 28.05s; Decl. =  $-69^{\circ} 16' 11''.64$ ; (J2000.0). SWS01 provides spectra which together cover the entire wavelength region between 2.38 – 45.2 $\mu$ m. However, as our models predict [Fe I] 24.05 $\mu$ m and [Fe II] 25.99 $\mu$ m to be by far the strongest emission

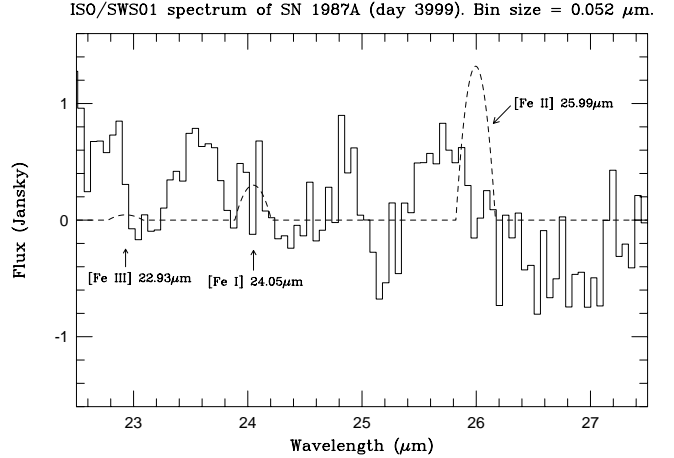


**Fig. 1.** ISO SWS/AOT1 Band 3 spectrum of SN 1987A on day 3999. The spectrum was reduced using interactive software (see text). The bin size was set to 0.052 $\mu$ m, in accordance with the instrumental resolution. Overlaid (dashed line) is the modeled line emission from model M2 (without photoionization) described in Table 2 and Sect. 3.2. To obtain the modeled line profiles we have assumed a maximum core velocity of 2000 km s<sup>-1</sup>, and that the emission is homogeneously distributed throughout the core (see Sect. 3.3). The modeled peak flux of [Fe II] 25.99 $\mu$ m corresponds to what is needed for a  $3\sigma$  detection.

lines from the supernova at this epoch (day 3999; see Sect. 3), we have concentrated on measuring the flux in the wavelength range including these two lines. This range, between 22.5 – 27.5 $\mu$ m, is covered by band 3D of SWS.

The reductions were made using the SWS Interactive Analysis software system (SIA) available at ISO Spectrometer Data Center (ISOSDC) at the Max Planck Institut für extraterrestrische Physik in Garching (MPE). The most recent set of calibration files equivalent to off-line processing (OLP/pipeline) version 7.0 was used. The interactive reduction allows special care to be given to dark subtractions, which is of particular interest when measuring low flux levels. Flat fielding was also applied, but we have not made any fringe corrections since the fringes at low flux levels disappear in the noise.

In Fig. 1 we present a fully reduced spectrum of SN 1987A for band 3D. Although the nominal instrumental resolution of SWS is  $R \approx 1000$ , the slowest SWS01 mode with speed 4 degrades this by a factor of 2. We have therefore averaged the spectrum with a bin size of 0.052 $\mu$ m, corresponding to 600–650 km s<sup>-1</sup> for the two lines of interest. As the lines could extend to well above  $\pm 2000$  km s<sup>-1</sup> this resolution should be sufficient to resolve the lines. However, neither [Fe I] 24.05 $\mu$ m nor [Fe II] 25.99 $\mu$ m are seen in the spectrum. The ‘features’ that do appear around  $\sim 23.5$  and 25.7 $\mu$ m are most likely due to instrumental effects, as they are rather robust in the sense that they appear in many detectors and in both up and down scans. They are

certainly not due to fringes, nor do we believe they are effects of pure noise. The zero level of the spectrum is well defined and a simple zero-order fit to the spectrum gives an RMS of  $\sim 0.47$  Jy over the range  $22.5 - 27.5\mu\text{m}$ .

Looking more closely at the spectral regions of the two lines, we have simply measured the RMS between  $23 - 25\mu\text{m}$  and  $25 - 27\mu\text{m}$  separately. Again, we used a zero-order fit to the smoothed spectrum. A zero-order fit should provide the most conservative way to estimate the ‘noise’ in our data. The resulting RMS values are  $\sim 0.34$  Jy and  $\sim 0.46$  Jy for [Fe I]  $24.05\mu\text{m}$  and [Fe II]  $25.99\mu\text{m}$ , respectively. This gives  $3\sigma$  upper limits of  $\sim 1.02$  Jy and  $\sim 1.38$  Jy for the peak of the profile of the two lines. These values do not change much even if we double the bin size.

SN 1987A was also observed in the SWS02 mode on three occasions (see Table 1). This mode provides scans over shorter wavelength ranges than the full SWS01 scans. We have reduced also the SWS02 data using SIA. While [Fe II]  $25.99\mu\text{m}$  was looked at on all three occasions (see Table 1), [Fe I]  $24.05\mu\text{m}$  was only looked at on June 8, 1996. The flux calibration for the SWS02 mode is in general more reliable than for SWS01 at a specific wavelength since dark exposures are taken immediately before and after the short SWS02 scans, and the sampling for the individual data points is better. However, the SWS02 observations in Table 1 cover only the range  $25.75 - 26.20\mu\text{m}$ , which could be just a fraction of the real line width. As the continuum level is therefore unknown, we have to rely on absolute flux calibrations, which are uncertain at the low flux levels of our data. Concentrating on the  $26\mu\text{m}$  line, we measure  $\sim 0.75$  Jy and  $\sim 0.62$  Jy for the two epochs with the longest exposures, May 26, 1996 and July 19, 1997, respectively. The accuracy of absolute fluxes for this wavelength regime at higher flux levels is  $< 20\%$  (ISOSWS Data Users Manual, v5.0), but for our very low flux levels,  $\sim 50\%$  is probably more fair.

Due to this uncertainty we can only say that our SWS02 flux estimates are consistent with the upper limits we obtain from the SWS01 measurement.

## 2.2. LWS Observations

Our LWS observations were made on 4 February, 1998. The full range of the LWS was scanned, i.e.,  $45 - 197\mu\text{m}$ . Standard reduction of the spectra using the ISO Spectral Analysis Package (ISAP) software resulted in the combined spectrum displayed in Fig. 2. Just as for the SWS observations, no emission was observed from the supernova. However, four unresolved emission lines from neighboring photoexcited gas were identified: [O I]  $63.2\mu\text{m}$ , [O III]  $51.8\mu\text{m}$ , [O III]  $88.4\mu\text{m}$  and [C II]  $158\mu\text{m}$ , with the fluxes  $(1.5 \pm 0.3) \times 10^{-12}$  erg  $\text{s}^{-1}$   $\text{cm}^{-2}$ ,  $(1.39 \pm 0.13) \times 10^{-11}$  erg  $\text{s}^{-1}$   $\text{cm}^{-2}$ ,  $(1.68 \pm 0.32) \times 10^{-11}$  erg  $\text{s}^{-1}$   $\text{cm}^{-2}$ , and  $(3.36 \pm 0.12) \times 10^{-12}$  erg  $\text{s}^{-1}$   $\text{cm}^{-2}$ , respectively. The lines sit on top of a broad continuum which peaks at

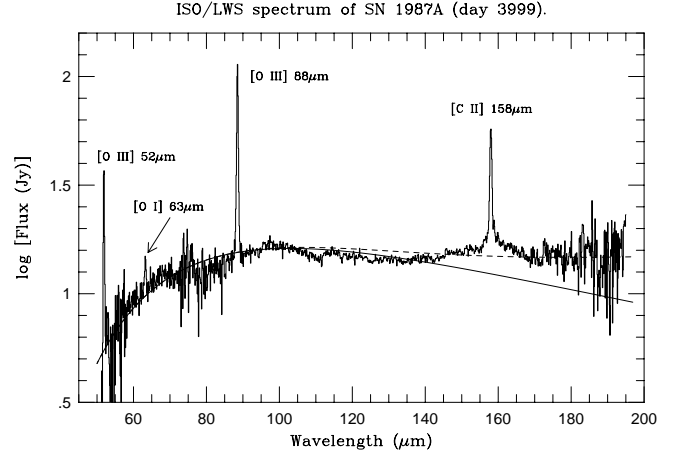


**Fig. 2.** ISO LWS spectrum of SN 1987A on day 3999. The continuum up to  $140\mu\text{m}$  can be fitted with a spectrum emitted by dust with a temperature of  $\sim 37$  K (solid smooth line). Longward of  $140\mu\text{m}$  a second component appears to add in. The temperature characterizing this component is  $\sim 10$  K. The combined emission is shown by the dashed line. See Sect. 2.2 and 4.3 for details.

$\sim 100\mu\text{m}$  at a level of  $(17 \pm 5)$  Jy, and which is only marginally weaker in the range  $\sim 145 - 165\mu\text{m}$ . The integrated continuum flux is  $(6 \pm 2) \times 10^{-10}$  erg  $\text{s}^{-1}$   $\text{cm}^{-2}$ , which for a distance of 50 kpc corresponds to a luminosity of  $(1.8 \pm 0.6) \times 10^{38}$  erg. It should be pointed out that the spatial region sampled has a large diameter ( $\sim 80''$ ), which at a distance of 50 kpc distance corresponds to  $\sim 19$  pc. We discuss the LWS results briefly in Sect. 4.3.

## 3. Interpreting the SWS observations

To understand what the upper limits on the iron lines in Sect. 2.1 mean, we have made model calculations. The models are described in Sect. 3.1, and we discuss the results from the calculations in Sect. 3.2

### 3.1. The model for line emission from the supernova

The code we have used for our theoretical calculations is described in detail in Kozma & Fransson (1998a), and here we will only give a brief summary of the model.

The thermal and ionization balances are solved time-dependently, as are also the level populations of the most important ions.

The ions included are H I-II, He I-III, C I-III, N I-II, O I-III, Ne I-II, Na I-II, Mg I-III, Si I-III, S I-III, Ar I-II, Ca I-III, Fe I-V, Co II, Ni I-II. The following ions are treated as multilevel atoms: H I, He I, O I, Mg I, Si I, Ca II, Fe I, Fe II, Fe III, Fe IV, Co II, Ni I, Ni II. The remaining lines are solved as 2-level atoms or as 4 – 6 level systems. For Fe I we include 121 levels, Fe II 191 levels, Fe III 112 levels and for Fe IV 45 levels. A total of approximately 6 400 lines are included in the calculations.

The radioactive isotopes included are  $^{56}\text{Ni}$ ,  $^{57}\text{Ni}$ , and  $^{44}\text{Ti}$ . These radioactive decays provide the energy source for the ejecta, and we calculate the energy deposition of gamma-rays and positrons solving the Spencer-Fano equation (see Kozma & Fransson [1992] for a more detailed description of our thermalization of the gamma-rays). We have assumed that the positrons deposit their energy locally, within the regions containing the newly synthesized iron.

We have included  $0.07 M_{\odot}$  of  $^{56}\text{Ni}$  (Sect. 1) and  $3.33 \times 10^{-3} M_{\odot}$  of  $^{57}\text{Ni}$ , which corresponds to a  $^{57}\text{Fe}/^{56}\text{Fe}$  ratio equal to two times the solar ratio. This mass of  $^{57}\text{Ni}$  gives a good fit to the bolometric light curve when the effects of freeze-out are taken into account (Fransson & Kozma 1993). It is also consistent with observations of [Fe II] and [Co II] IR lines (Varani et al. 1990; Danziger et al. 1991), observations of the  $^{57}\text{Co}$  122 keV line (Kurfess et al. 1992), and theoretical nucleosynthesis calculations (Woosley & Hoffman 1991). In our ‘standard’ model we have used  $1.0 \times 10^{-4} M_{\odot}$  of  $^{44}\text{Ti}$  (e.g., Kumagai et al. 1991; Timmes et al. 1996). We have also made calculations with  $M(^{44}\text{Ti}) = 0.5 \times 10^{-4} M_{\odot}$  and  $M(^{44}\text{Ti}) = 2.0 \times 10^{-4} M_{\odot}$ .

Until recently, the lifetime of  $^{44}\text{Ti}$  has been very poorly known. In our calculations we have used an e-folding time of 78 years thought to be a representative value to those found from experiments. However, while completing our calculations, we were informed about the recent measurements mentioned in Sect. 1 (S. Nagataki, private communication). The new, and accurate value,  $87.0 \pm 1.9$  years, is close to what we have used, but decreases the instantaneous radioactive energy input from the  $^{44}\text{Ti}$  decay by  $\lesssim 12\%$ . This systematic error, shifting our estimated value of  $M(^{44}\text{Ti})$  upward by a similar amount, has been included in the error analysis in Sect. 4.1.

As input for the calculations we have adopted the abundances from the 10H explosion model (Woosley & Weaver 1986; Woosley 1988). Spherically symmetric geometry has been assumed, with shells containing the major composition regions as given by the explosion model. We have used the same distribution of shells as in Kozma & Fransson (1998a) where hydrogen is mixed into the core. The iron-rich core is assumed to extend out to  $2000 \text{ km s}^{-1}$ , outside of which we attach a hydrogen envelope, out to  $6000 \text{ km s}^{-1}$ .

For the line transfer we have used the Sobolev approximation. This is justified for well-separated lines in an expanding medium. However, especially in the UV, there are many overlapping lines, and one can expect UV-scattering to be important. The importance of line scattering decreases with time as the optical depths decrease. The effect of line scattering is to alter the emergent UV-spectrum, but it also affects the UV-field within the ejecta. The ionization of elements with low ionization potential is sensitive to the UV-field. During scattering the UV photons are shifted towards longer wavelengths, both due to a pure Doppler shift, but also because of the increased probability

of splitting the UV-photons into several photons of longer wavelengths. A more accurate treatment of the line scattering is therefore expected to decrease the importance of photoionization. For the modeling of [Fe II]  $25.99\mu\text{m}$ , the photoionization of Fe I to Fe II is likely to introduce the largest uncertainty. To check the importance of this effect we have in some models simply switched off the photoionization. A more comprehensive line transfer modeling is discussed in KF99.

### 3.2. Model calculations

The results of our calculations can be seen in Table 2. We tabulate line fluxes for four strong lines for three values of  $M(^{44}\text{Ti})$ :  $5 \times 10^{-5}$  (M1),  $1 \times 10^{-4}$  (M2) and  $2 \times 10^{-4} M_{\odot}$  (M3). For each value of  $M(^{44}\text{Ti})$  we show results for models with and without photoionization. In all six models a simple form of dust absorption was assumed (Kozma & Fransson 1998b). The line fluxes in Table 2 are for a box line profile between  $\pm 2000 \text{ km s}^{-1}$ , and assuming a distance to the supernova of 50 kpc.

From Table 2 it is evident that [Fe II]  $25.99\mu\text{m}$  is by far the strongest line in our simulations, and that its flux scales roughly linearly with  $M(^{44}\text{Ti})$ , as expected from Sect. 1. From power-law fits to the results of the calculations described in Table 2, we obtain  $f_{26\mu\text{m}} \propto M(^{44}\text{Ti})^{1.13}$  when photoionization is included, and nearly the same without photoionization ( $f_{26\mu\text{m}} \propto M(^{44}\text{Ti})^{1.12}$ ). The second strongest line is [Fe I]  $24.05\mu\text{m}$ . Its dependence on  $M(^{44}\text{Ti})$  is weaker:  $f_{24\mu\text{m}} \propto M(^{44}\text{Ti})^{0.56}$  and  $f_{24\mu\text{m}} \propto M(^{44}\text{Ti})^{0.73}$ , respectively. Other lines from SN 1987A are far too weak for our ISO observations.

The stronger dependence of  $f_{26\mu\text{m}}$  on  $M(^{44}\text{Ti})$  than for  $f_{24\mu\text{m}}$  is due to ionization: while a higher  $M(^{44}\text{Ti})$  boosts the relative fraction of Fe II,  $X_{\text{FeII}}$ , the relative fraction of Fe I,  $X_{\text{FeI}}$ , decreases. For example, in models with photoionization, the average value of  $X_{\text{FeII}}$  in the Fe-rich gas increases from  $\sim 0.32$  to  $\sim 0.55$  when  $M(^{44}\text{Ti})$  is increased from  $5 \times 10^{-5}$  to  $2 \times 10^{-4}$ , while  $X_{\text{FeI}}$  decreases from  $\sim 0.65$  to  $\sim 0.36$ . The fact that the  $26\mu\text{m}$  line is so much stronger than the  $24\mu\text{m}$  line despite the roughly similar relative fractions of Fe I and Fe II is just a result of the much larger collision strength of the Fe II line than for [Fe I]  $24.05\mu\text{m}$ .

Table 2 shows that switching off photoionization does not have a dramatic effect on the line fluxes. In the case of M2,  $f_{26\mu\text{m}}$  decreases by  $\sim 15\%$  and  $f_{24\mu\text{m}}$  increases by  $\sim 28\%$  when we turn off photoionization, simply due to a minor shift in ionization between Fe I and Fe II. As we will discuss in Sect. 4.1, there are other uncertainties which are of the same magnitude.

### 3.3. Mass of $^{44}\text{Ti}$ from [Fe II] $25.99\mu\text{m}$

With our results it is straightforward to estimate the upper limit on  $M(^{44}\text{Ti})$ . Using  $f_{26\mu\text{m}} \lesssim 1.38 \text{ Jy}$  from Sect.

**Table 2.** Modeled line flux in Jy at 4000 days<sup>a,b</sup>

Line	M1 <sup>c</sup>	M2 <sup>d</sup>	M3 <sup>e</sup>
[Fe I] 24.047 $\mu$ m	0.11 (0.12)	0.16 (0.20)	0.23 (0.33)
[Fe II] 25.995 $\mu$ m	0.45 (0.40)	1.03 (0.88)	2.19 (1.89)
[Fe II] 35.359 $\mu$ m	0.01 (0.01)	0.04 (0.04)	0.12 (0.11)
[Fe III] 22.930 $\mu$ m	0.01 (0.01)	0.03 (0.03)	0.11 (0.11)

<sup>a</sup> Distance = 50 kpc. Box line profile of width  $\pm 2000$  km s<sup>-1</sup>.

<sup>b</sup> For values in parantheses photoionization has been excluded.

<sup>c</sup>  $M(^{44}\text{Ti}) = 5 \times 10^{-5} M_{\odot}$

<sup>d</sup>  $M(^{44}\text{Ti}) = 1 \times 10^{-4} M_{\odot}$

<sup>e</sup>  $M(^{44}\text{Ti}) = 2 \times 10^{-4} M_{\odot}$

2.1, and our power-law fit to the results in Table 2 (Sect. 3.2), we find an upper limit which is  $M(^{44}\text{Ti}) \lesssim 1.3(1.5) \times 10^{-4} M_{\odot}$  with (without) photoionization included. These masses are for a box-shaped line profile, and therefore provide conservative limits. However, there is good reason to believe that the line profile should be similar to those for the lines observed by Haas et al. (1990)  $\sim 400$  days after the explosion. The strongest line observed by Haas et al. was [Fe II] 17.94 $\mu$ m and it had  $v_{\text{FWHM}} = (2900 \pm 80)$  km s<sup>-1</sup>. Although it peaked just short off +1000 km s<sup>-1</sup>, and thus was not symmetric around the rest velocity of the supernova, it had the general appearance of the expected line profile formed by a filled sphere with constant emission throughout the sphere. For a sphere extending out to 2000 km s<sup>-1</sup>, the peak is 1.5 times higher than for the box profile used in Table 2 (which is valid for a hollow sphere), and  $v_{\text{FWHM}} = 2828$  km s<sup>-1</sup>. Using such a line profile in our upper limits on  $M(^{44}\text{Ti})$ , we instead obtain  $M(^{44}\text{Ti}) \lesssim 0.9(1.0) \times 10^{-4} M_{\odot}$  with (without) photoionization included. Within the framework of our modeling, a conservative limit (i.e., the case when photoionization is unimportant) for a plausible line profile is therefore  $M(^{44}\text{Ti}) \lesssim 1.0 \times 10^{-4} M_{\odot}$ . In Fig. 1, we have included the expected line emission for such a model with this limiting mass of  $^{44}\text{Ti}$ . We will evaluate this limit on  $M(^{44}\text{Ti})$  in Sect. 4.1.

## 4. Discussion

### 4.1. Uncertainties in the modeling

There are several uncertainties involved in our modeling of the line fluxes. We have already checked the effect of the lifetime of  $^{44}\text{Ti}$  (Sect. 3.1). We have also studied the effect of photoionization, and found that it introduces rather mild uncertainties. A similar level of uncertainty is due to the distance to the supernova. This is still inaccurate to the level of 5 – 10% (Lundqvist & Sonneborn 1999; Walker 1999), which means an uncertainty in the line flux of  $\sim 10 - 20\%$ .

Atomic data of iron are notoriously difficult to calculate accurately. This is therefore another source of error in our modeling, especially for individual lines. Most important for the 26 $\mu$ m line is the collision strength of that transition,  $\Omega_{26\mu\text{m}}$ . One normally assigns an uncertainty in the collision strength for the strongest iron lines to  $\sim 30\%$  (e.g., Verner et al. 1999). In our models we have used  $\Omega_{26\mu\text{m}} = 5.8$  (Zhang & Pradhan 1995). To study the effect in detail we have tested a model with  $M(^{44}\text{Ti}) = 10^{-4} M_{\odot}$  and  $\Omega_{26\mu\text{m}} = 2.9$ . We find that there is not a linear scaling between  $f_{26\mu\text{m}}$  and  $\Omega_{26\mu\text{m}}$ , as one might naively believe. Instead, we find from linear interpolation that a 30% decrease in collision strength gives a  $\sim 17\%$  lower  $f_{26\mu\text{m}}$ , and a correspondingly higher estimate of  $M(^{44}\text{Ti})$ . The reason for this is that the gas is slightly hotter in the model with reduced collision strength, boosting the exponential term in the collisional rate so that it somewhat counteracts the reduced collision strength. We have recently found out (A. Pradhan, private communication) that the preferred value for  $\Omega_{26\mu\text{m}}$  at the low temperatures in SN 1987A is most likely closer to  $\sim 7.0$ , i.e., higher than we have used. Despite this, we have generously assigned an uncertainty of 15% (upwards) in  $M(^{44}\text{Ti})$  due to atomic data.

Another source of uncertainty could be the explosion model used. In these calculations we have used the abundances from the 10H explosion model. A comparison between the two models 10H (Woosley & Weaver 1986; Woosley 1988) and 11E1 (Shigeyama et al. 1988) was done in Kozma & Fransson (1998b). There it was found that the iron lines are not sensitive to the explosion model used, because the iron core mass is the same in both models. The iron core mass is set by the amount of  $^{56}\text{Ni}$  which is accurately determined from the bolometric light curve. The choice of explosion model thus does not seem to be a major source of uncertainty when modeling these iron lines.

In our calculations we assume a local deposition of the positrons originating from the radioactive decays of  $M(^{44}\text{Ti})$ . We believe this is a good approximation since optical and near-IR light curves of Fe I and Fe II lines show that trapping must occur (Chugai et al. 1997; Kozma & Fransson 1998b). Actually, there is no obvious sign of a leakage of positrons, neither from broad-band lightcurves (KF99), nor from the optical Fe I lines at 6300 Å until the last data point at 3597 days in Kozma (1999). Although the trapping may well be fully complete, we have assigned an error to this assumption by 15%.

Another approximation in our models is the assumption of a homogeneous density in each Fe-rich shell of the model core. To test the sensitivity to this assumption, we have run a model similar to M2, with photoionization included (see Table 2), but where we have divided the mass in the Fe-rich ejecta into two components of equal mass but with different densities. The denser component is set to be nearly five times more dense than the other. Despite the significantly different density distribution in this

model compared to that in M2, the differences in  $f_{26\mu\text{m}}$  and  $f_{24\mu\text{m}}$  between the models are small. Instead of the values listed in Table 2, the fluxes in the two-component model are 0.98 and 0.20 Jy, respectively, i.e.,  $f_{26\mu\text{m}}$  differs by only  $\sim 5\%$  compared to that in M2. This indicates that the model assumption of a homogeneous density in each Fe-rich shell does not introduce a major uncertainty.

Finally, screening and cooling by dust are potential sources of error in our models. The effects of dust are examined in Kozma & Fransson (1998ab). The screening we use is discussed in Kozma & Fransson (1998b), and is based on estimates by Lucy et al. (1991) and Wooden et al. (1993). Dust from pure iron is unlikely to form, as that would cool and block out all iron line emission once the dust has formed. On the contrary, there is a wealth of iron lines from the core at late times. KF99 and Kozma (1999) find good agreement between modeled and observed broad-band lightcurves for  $t \lesssim 3270$  days and spectra at 2870 days. As was pointed out also for the positron leakage, the models are also able to reproduce optical Fe I lines at even later epochs. Based on this, we believe dust effects are small enough to neglect in our estimate of  $M(^{44}\text{Ti})$ .

None of the model approximations we have used appears to be uncertain enough to allow  $f_{24\mu\text{m}}$  to be of the same magnitude as  $f_{26\mu\text{m}}$ . The best estimate of  $M(^{44}\text{Ti})$  (within the framework of our modeling) should therefore come solely from  $f_{26\mu\text{m}}$ . To estimate the combined error of  $f_{26\mu\text{m}}$  due to all model approximations (except for the dust distribution in the ejecta), we adopt the uncertainties 15%, 15%, 15% and 5% for photoionization, distance, atomica data and clumping, respectively. For the choice of input model and positron leakage we adopt 15% each. This gives a combined uncertainty which is  $\sim 34\%$ . On top of this we must add the maximum systematic error of 12% discussed in Sect. 3.1 for the lifetime of  $^{44}\text{Ti}$ . With the line profile discussed in Sect. 3.3, we therefore arrive at an upper limit on  $M(^{44}\text{Ti})$  which is  $\simeq 1.5 \times 10^{-4} M_{\odot}$ . We note that this limit excludes the upper ends of the allowed ranges of  $M(^{44}\text{Ti})$  found by Chugai et al. (1997) and KF99 (see Sect. 1). Combining our limit with the preliminary results of KF99 for the broad-band photometry, a likely range for  $M(^{44}\text{Ti})$  is  $(0.5 - 1.5) \times 10^{-4} M_{\odot}$ . We emphasize, however, that the lower limit of this range is probably more uncertain than the upper (for the reasons mentioned in Sect. 1), which is indeed indicated by the preliminary analysis of Borkowski et al. (1997).

#### 4.2. Implications of the derived mass of $^{44}\text{Ti}$

Models for the yield of  $^{44}\text{Ti}$  give quite different results. This is most likely due to how the explosion is generated in the models, and how fallback onto the neutron star is treated. Timmes et al. (1996; see also Woosley & Weaver 1995) use a piston to generate the explosion, and they account for fallback in a rather self-consistent way. In their

model with zero-age mass  $M_{\text{ZAMS}} = 20 M_{\odot}$  (i.e., corresponding to SN 1987A) the mass of the initially ejected  $^{44}\text{Ti}$  is  $1.2 \times 10^{-4} M_{\odot}$ , but of this only  $1.4 \times 10^{-5} M_{\odot}$  escapes after fallback. This is less than we argue for in Sect. 4.1, and could suggest that fallback was not important for SN 1987A, though we caution again that the lower limit found by KF99 (see also Kozma 1999) may not be very strict. If fallback is unimportant the ejected amounts of  $^{56}\text{Ni}$  and  $^{57}\text{Ni}$  would be too high in this model, typically by a factors of  $\sim 2 - 4$ , judging from the effects of fallback in the  $25 M_{\odot}$  model in Woosley & Weaver (1995). It should be emphasized that the variation of  $M(^{44}\text{Ti})$  with  $M_{\text{ZAMS}}$  in Timmes et al. (1996) is complex, and that for models with  $M_{\text{ZAMS}} = 18 M_{\odot}$  and  $M_{\text{ZAMS}} = 22 M_{\odot}$ , the calculated  $M(^{44}\text{Ti})$  comes within the range we propose, albeit close to our lower limit.

The models of Thielemann et al. (1996) simulate the explosion by depositing thermal energy in the core, and they insert the mass cut artificially so that the right amount of ejected  $^{56}\text{Ni}$  is produced. (This effectively means that fallback is included also in these models.) Simulating the explosion in this way ensures larger entropy and thus more alpha-rich freeze-out than in Woosley & Weaver (1995). Accordingly, the ratio  $M(^{44}\text{Ti})/M(^{56}\text{Ni})$  (where  $M(^{56}\text{Ni})$  is the mass of ejected  $^{56}\text{Ni}$  that does not fall back) is higher in the models of Thielemann et al. than in piston-driven simulations. For example, in the  $20 M_{\odot}$  model of Thielemann et al. (1996)  $M(^{56}\text{Ni}) \approx 0.074 M_{\odot}$ ,  $M(^{57}\text{Ni}) \approx 2.9 \times 10^{-3} M_{\odot}$  and  $M(^{44}\text{Ti}) \approx 1.7 \times 10^{-4} M_{\odot}$ , with  $M(^{57}\text{Ni})$  defined in the same way as  $M(^{56}\text{Ni})$  and  $M(^{44}\text{Ti})$ . The values of  $M(^{56}\text{Ni})$  and  $M(^{57}\text{Ni})$  are close to what have been inferred for SN 1987A (Suntzeff & Bouchet 1990; Fransson & Kozma 1993). The titanium mass is slightly larger than the upper limit of the range we estimate in Sect. 4.1. So, while our estimate of  $M(^{44}\text{Ti})$  cannot rule out with certainty any of the two methods used for the explosion (piston-driven or heat generated), our results could indicate that an intermediate method should be used (see also the discussion on this in Timmes et al. 1996). From models of the chemical evolution of the Galaxy, and especially the solar abundance of  $^{44}\text{Ca}$ , a value for  $M(^{44}\text{Ti})$  closer to that of Thielemann et al. (1996) may be more correct, at least for supernovae in general.

In this context we note that a higher value of  $M(^{44}\text{Ti})$  is produced in asymmetric explosions (Nagataki et al. 1998). The method of calculation employed by Nagataki et al. (see Nagataki et al. 1997) is similar to that in Thielemann et al. (1996), though the models of Nagataki et al. allow for 2-D instead of just 1-D. With no asymmetry, the models of Nagataki et al. produce  $M(^{44}\text{Ti}) \sim 6 \times 10^{-5} M_{\odot}$  for an explosion similar to SN 1987A, when the mass cut has been trimmed to  $M(^{56}\text{Ni}) \approx 0.07 M_{\odot}$ . This is significantly less than Thielemann et al. (1996) despite the similar method of modeling. Applying an asymmetry by a factor of 2 between the equator and the poles, the explosion

energy becomes concentrated toward the equator resulting in relatively stronger alpha-rich freeze-out, which increases  $M(^{44}\text{Ti})$  to  $\sim 2 \times 10^{-4} M_{\odot}$  (for  $M(^{56}\text{Ni}) \approx 0.07 M_{\odot}$ ). This is outside our observationally determined range and could indicate that asymmetry was not extreme in SN 1987A, especially if  $M(^{44}\text{Ti})$  is close to the limit derived by Borkowski et al. (1997). We note that a piston-driven calculation could perhaps allow for asymmetry, as such models give very small values of  $M(^{44}\text{Ti})$  in 1-D.

A direct way to estimate  $M(^{44}\text{Ti})$  in supernovae is to observe the gamma-ray emission from the radioactive decay of  $^{44}\text{Ti}$ . The 1.156 MeV line associated with the decay of  $^{44}\text{Ti}$  has only been detected in two supernova remnants (and no supernovae): Cas A (Iyudin et al. 1994; The et al. 1996) and the newly discovered gamma-ray/X-ray source GRO J0852-4262/RX J0852.0-4622 (Iyudin et al. 1998; Aschenbach 1998). While  $M(^{44}\text{Ti})$  in the latter is not yet well-known,  $M(^{44}\text{Ti})$  in Cas A was  $1.7^{+0.6}_{-0.5} \times 10^{-4} M_{\odot}$  (Görres et al. 1998). In the models of Nagataki et al. (1998), the value of  $M(^{44}\text{Ti})$  at the upper end of this range would indicate that Cas A exploded asymmetrically. Our estimate of  $M(^{44}\text{Ti})$  in Sect. 4.1 does not seem to indicate a high degree of asymmetry for SN 1987A, but an independent measurement of its 1.156 MeV line may be needed to be more conclusive on this point. To detect this emission from SN 1987A, instruments like INTEGRAL (Leising 1994) are required.

#### 4.3. Interpretation of LWS observations

The two [O III] lines observed (see Sect. 2.2 and Fig. 2) can be used to estimate the average density of the emitting gas. We have used a multi-level atom to do this, using the atomic data of Mendoza (1983), Osterbrock (1989) and Aggarwal (1993). Assuming a temperature of  $10^4$  K, we obtain a mean electron density of  $120 \pm 75 \text{ cm}^{-3}$  in the [O III] emitting gas.

The continuum can be fitted with a spectrum of the form  $F_{\lambda} \propto B_{\lambda}(T)(1 - \exp(-\tau_D))$ , where  $\tau_D$  is the dust optical depth. With a functional form of  $\tau_D = \tau_{0.55}(0.55/\lambda)^{\alpha}$  (where  $\lambda$  is in microns) we obtain a best fit with  $T \simeq 37$  K,  $\tau_{0.55} \simeq 0.74$  and  $\alpha \simeq 0.83$ . The fit (see Fig. 2) works well up to  $\simeq 140 \mu\text{m}$ , where an extra source appears to add in. This could indicate the presence of cold dust. Assuming the same functional form for this emission as for the 37 K component, the temperature of the cold component is close to 10 K.

## 5. Conclusions

We have looked at SN 1987A with ISO SWS/LWS. The supernova was not detected in any of the spectra. In particular, we have derived upper limits for the fluxes of [Fe I]  $24.05 \mu\text{m}$  and [Fe II]  $25.99 \mu\text{m}$ , and made time dependent calculations for the late line emission from the supernova. We have assessed various uncertainties to

the models, and for a plausible line profile we then find an upper limit on the mass of ejected  $^{44}\text{Ti}$ ,  $M(^{44}\text{Ti}) \simeq 1.5 \times 10^{-4} M_{\odot}$ . Together with the preliminary results of KF99 this brackets the ejected mass of  $^{44}\text{Ti}$  to the range  $M(^{44}\text{Ti}) = (0.5 - 1.5) \times 10^{-4} M_{\odot}$ , which is close to the yield of  $^{44}\text{Ti}$  in models of the explosion by Woosley & Weaver (1995), Thielemann et al. (1996) and Nagataki et al. (1997). The lower limit is probably less stringent than the upper, as indicated by the results of Borkowski et al. (1997). A more direct limit on  $M(^{44}\text{Ti})$  can be made when instruments measuring the gamma-ray line emission from the  $^{44}\text{Ti}$  decay will be available.

The only emission our ISO observations detect is from gas and dust in the direction toward the supernova. In particular, the [O III]  $51.8 \mu\text{m}$  and [O III]  $88.4 \mu\text{m}$  lines indicate a gas density of  $120 \pm 75 \text{ cm}^{-3}$ , and the dust continuum can be explained by a temperature of  $\sim 37$  K. A second dust component with  $\sim 10$  K may also be present.

*Acknowledgements.* We thank Claes Fransson for comments and stimulating discussions, and Bruno Leibundgut and the referee Tino Oliva for comments on the manuscript. We also thank Shigehiro Nagataki and Anil Pradhan for updating us on nuclear and atomic data, respectively. We acknowledge support from the ISOSDC at MPE. ISAP is a joint development by the LWS and SWS Instrument Teams and Data Centers. Contributing institutes are CESR, IAS, IPAC, MPE, RAL and SRON. This research was supported by the Swedish Natural Science Research Council, the Swedish National Space Board, and the Knut & Alice Wallenberg Foundation. A.P.S.C. is grateful for support from NASA grants NAG5-3319 and NAG5-3502.

## References

- Aggarwal K.M. 1993, ApJS, 85, 197
- Ahmad I., Bonino G., Cini Castagnoli, G., et al. 1998, Phys. Rev. Lett., 80, 2550
- Aschenbach B. 1998, Nature, 396, 141
- Borkowski K.J., de Kool M., McCray R., Wooden D.H. 1997, BAAS, 29, 1269
- Bouchet P., Danziger I.J., Gouffes C., et al. 1996, in IAU Coll. No. 45, Supernovae and Supernova Remnants, ed. R. McCray & Z. Wang (CUP: Cambridge), 201
- Chugai N.N., Chevalier R.A., Kirshner R.P., Challis P.M. 1997, ApJ, 483, 925
- Clegg P.E., Ade P.A.R., Armand C., et al. 1996, A & A, 315, L38
- Danziger I.J., Lucy L.B., Bouchet P., Gouffes C. 1991, in Supernovae, ed. S.E. Woosley (Springer: New York), 69
- de Graauw T., Haser L.N., Beintema D.A., et al. 1996, A & A, 315, L49
- Fransson C., Kozma C. 1993, ApJ, 408, L25
- Fransson C., Kozma C. 1999, in Proc. CTIO/ESO/LCO Workshop, SN 1987A: Ten Years After, ed. M. Phillips & N. Suntzeff, A.S.P. Conference Series, in press (<ftp://www.astro.su.se/pub/supernova/preprints.html>)
- Görres J., Meissner J., Schatz H., et al. 1998, Phys. Rev. Lett., 80, 2554

- Haas M.R., Erickson E.F., Lord S.D., et al. 1990, *ApJ*, 360, 257
- Iyudin A.F., Diehl R., Bloemen, H., et al. 1994, *A & A*, 284, L1
- Iyudin A.F., Schönfelder V., Bennett K., et al. 1998, *Nature*, 396, 142
- Kessler M.F., Steinz J.A., Anderegg M.E., et al. 1996, *A & A*, 315, L27
- Kozma C. 1999, in *Proc. Future Directions in Supernova Research: Progenitors to Remnants*, ed. S. Cassisi & P. Mazzali, to be published in *Mem. Soc. Astr. Ital.* (astro-ph/9903405)
- Kozma C., Fransson C. 1992, *ApJ*, 390, 602
- Kozma C., Fransson C. 1998a, *ApJ*, 496, 946
- Kozma C., Fransson C. 1998b, *ApJ*, 497, 431
- Kumagai S., Shigeyama T., Hashimoto M., Nomoto K. 1991, *A&A*, 243, L13
- Kurfess J.D., Johnson W.N., Kinzer R.L., et al. 1992, *ApJ*, 399, L137
- Leising M.D. 1994, *ApJS*, 92, 495
- Lucy L.B., Danziger I.J., Gouiffes C., Bouchet P. 1991, in *Proc. Supernovae*, ed. S.E. Woosley (Springer Verlag), 82
- Lundqvist P., Sonneborn G. 1999, in *Proc. CTIO/ESO/LCO Workshop, SN 1987A: Ten Years After*, ed. M. Phillips & N. Suntzeff, A.S.P. Conference Series, in press (astro-ph/9707144)
- Mendoza C. 1983, in *IAU Symp. 103, Planetary Nebulae*, ed. D.R. Flower (Dordrecht: Reidel), 143
- Nagataki S., Hashimoto M., Sato K., Yamada S. 1997, *ApJ*, 486, 1026
- Nagataki S., Hashimoto M., Sato K., et al. 1998, *ApJ*, 492, L45
- Osterbrock D.E. 1989, *Astrophysics of Gaseous Nebulae and Active Galactic Nuclei*, University Science Books
- Shigeyama T., Nomoto K., Hashimoto M. 1988, *A&A*, 196, 141
- Suntzeff N.B., Bouchet P. 1990, *AJ*, 99, 650
- Suntzeff N.B., Phillips M.M., Elias J.H., et al. 1992, *ApJ*, 384, L33
- The L.-S., Leising M.D., Kurfess J.D. 1996, *A&AS*, 120, 357
- Thielemann F.-K., Nomoto K., Hashimoto M. 1996, *ApJ*, 460, 408
- Timmes F.X., Woosley S.E., Hartmann D.H., Hoffman R.D. 1996, *ApJ*, 464, 332
- Varani G.-F., Meikle W.P.S., Spyromilio J., Allen D.A. 1990, *MNRAS*, 245, 570
- Verner E.M., Verner D.A., Korista K.T., et al. 1999, *ApJS*, 102, 101
- Walker A.R. 1999, in *Post Hipparcos Cosmic Candles*, ed. F. Caputo & A. Heck, (Kluwer: Dordrecht), in press (astro-ph/9808336)
- Wooden D.H., Rank D.M., Bregman J.D., et al. 1993, *ApJS*, 88, 477
- Woosley S.E. 1988, *ApJ*, 330, 218
- Woosley S.E., Hoffman R.D. 1991, *ApJ*, 368, L31
- Woosley S.E., Weaver T.A. 1986, *ARA&A*, 24, 205
- Woosley S.E., Weaver T.A. 1995, *ApJS*, 101, 181
- Woosley S.E., Pinto P.A., Ensmann L. 1988, *ApJ*, 324, 466
- Woosley S.E., Pinto P.A., Hartmann D. 1989, *ApJ*, 346, 395
- Zhang H.L., Pradhan A.K. 1995, *A&A*, 293, 953